Taylor & Francis
Taylor & Francis Group

Automatika

Journal for Control, Measurement, Electronics, Computing and Communications

ISSN: 0005-1144 (Print) 1848-3380 (Online) Journal homepage: https://www.tandfonline.com/loi/taut20

Implementation of solar PV system unified ZSI-based dynamic voltage restorer with U-SOGI control scheme for power quality improvement

T. Jayakumar & Albert Alexander Stonier

To cite this article: T. Jayakumar & Albert Alexander Stonier (2020) Implementation of solar PV system unified ZSI-based dynamic voltage restorer with U-SOGI control scheme for power quality improvement, Automatika, 61:3, 371-387, DOI: 10.1080/00051144.2020.1760591

To link to this article: https://doi.org/10.1080/00051144.2020.1760591

Published online: 12 May 2020.

AUTOMATIKA
2020, VOL. 61, NO. 3, 371–387
https://doi.org/10.1080/00051144.2020.1760591

REGULAR PAPER

OPEN ACCESS Check for updates

Implementation of solar PV system unified ZSI-based dynamic voltage restorer with U-SOGI control scheme for power quality improvement

T. Jayakumar [a] and Albert Alexander Stonier [b]

[a]Department of Electrical and Electronics Engineering, Nandha Engineering College, Erode, India; [b]Department of Electrical and Electronics Engineering, Kongu Engineering College, Erode, India

ABSTRACT

The main challenge in today's power system is to supply continuous, reliable power and satisfy the high demand. The incorporation of renewable energy sources into the utility grid system can be accomplished. However, the renewable sources are intermittent in nature and the loads work dynamically and cause imbalances to the system voltage within an immediate time. Intermittent renewable sources affect the voltage of the power grid system. Photovoltaic (PV) power generation with Z-source inverter (ZSI)-based dynamic voltage restorer (DVR) is used to avoid that. For step-up low DC voltage to required AC voltage for the compensation of the voltage disturbance, ZSI with the energy storage impedance network is used. DC-DC converters connect the PV cell and the battery storage to the impedance source network. This article also incorporates an upgraded second-order generalized integrator (U-SOGI) control system for the generation of reference voltage signals. The U-SOGI control reference voltage generation approach greatly improves system performance and decreases the harmonic voltage. The voltage-related problems in the system connected to the utility grid are mitigated with DVR. In different load and source conditions, the PV generation with DVR performance is verified by the digital simulation and experimental prototype.

ARTICLE HISTORY
Received 18 January 2020
Accepted 20 April 2020

KEYWORDS
Dynamic voltage restorer; second-order generalized integrator; solar photovoltaic; Z-source Inverter; Total harmonic distortion

Nomenclature

PV	photovoltaic
ZSI	Z- source inverter
DVR	dynamic voltage restorer
U-SOGI	upgraded second-order generalized integrator
I_{sc}	short circuit current
V_{oc}	open-circuit voltage
I_{Ph}	photocurrent (A)
I_{PV}	PV current (A)
V_{PV}	solar PV voltage (V)
K	Boltzmann constant
I_D	diode saturation current (A)
T_n	PV cell reference temperature (°C)
n	ideality factor of the diode
Ns	number of series-connected PV cells
q	electron charge (coulombs)
R_S	series resistance (Ω)
V^*_{Cd}, V^*_{Cq}, V^*_{C0}	reference compensation voltage in $dq0$ reference frame
V^*_{Ca}, V^*_{Cb}, V^*_{Cc}	reference compensation voltage in abc reference frame
PCC	point of Common Coupling
FPGA	field-programmable-gate-array
R-L	resistive-inductive
K_p, K_i, K_d	proportional, integral and derivative gains

1. Introduction

The electricity demand for loads has increased every day in India, due to technological advancement, population growth, and industry growth. The incorporation of renewable sources into the existing electrical energy system will meet demand. With the introduction of renewable sources incorporated into the present energy system, the deficit in demand is decreasing every year. Both isolated and grid-connected electrical networks, wind and solar power sources play a significant role. In contrast to other sources of renewable energy, PV incorporation plays a vital role in the electrical distribution system. Nevertheless, solar energy has an intermittent nature and affects both the grid and the reactive load [1]. Due to its intermittent existence, PV power does not provide a continuous power supply [2]. With the introduction of battery storage systems, the intermediation issue is avoided. The combination of these energy sources provides versatile energy and satisfies the necessary long-term peak demand. In the

CONTACT T. Jayakumar tjayakumaar@yahoo.com Department of Electrical and Electronics Engineering, Nandha Engineering College, Perundurai, Erode, 638 052, Tamil Nadu, India

This article has been republished with minor changes. These changes do not impact the academic content of the article.

distribution system, this hybrid generation plays the main role in meeting the demand for load [3]. In the power distribution system, this PV power generation plays the main role in meeting the demand for load [4].

The PV system is fed by the power converter to the distribution grid to provide a continuous power supply [5–7]. Nevertheless, the simultaneous switching of non-linear loads disrupts the connected grid system. This can cause an imbalance of the line voltage, vibration, voltage falls, voltage swell, spike, grid failure and harmonics that can damage sensitive loads. Customized equipment, including DVR, Distribution Static Synchronous Compensator (DSTATCOM) and Unified Power Quality Conditioner (UPQC), used in the distribution system protects the critical loads [8]. DVR is the perfect solution to solving voltage-related problems in customer power devices as it is cost-effective. The cost-effective DVR is the most attractive among customer power devices and provides the solution for solving voltage-related problems [9,10]. The DVR is a static converter and is realized from the converter of the voltage source. A DVR is built in series through the interconnected series transformer with a power distribution line. The DVR restores voltage in unbalanced or voltage loss conditions in series with a supply line. In the application of Doubly Fed Induction Generator (DFIG)-based wind turbine in a fault ride-through capability, DVR with a storage system is implemented for mitigation of voltage sag and manages the DC link voltage [11]. To protect the sensitive load, DVR with a self-tuned fuzzy-PI controller is provided to maximize the power flow with improved power factor [12]. Voltage sag is compensated by using a DVR with second degrees of freedom of the resonant control scheme [13]. To secure the sensitive load, hybrid energy storage system based DVR is introduced with a sensitive load [14]. Transformerless DVR (TDVR) with a predictive based control algorithm is used through the buck-boost AC-AC converter to compensate for the voltage sag and swell [15]. DVR with fault current limiter is utilized for optimizing the power flow with power factor improvement to protect the sensitive load [16]. Using dual p-q theory, optimized power flow is done via DVR and a passive filter [17].

The DVR alone cannot sustain the load voltage continuously during peak demand. A primary supply of energy is required to meet the highest demand and to sustain the load voltage in the distribution system. With the incorporation of renewable resources, continuous demand for the load is met. The DVR is fed with PV systems connected to the grid, to prevent such power-conditioning issues in distribution networks. The DVR does not need a separate source to restore system voltage in the proposed PV generating system with a battery storage unit. The DVR input is integrated directly with the DC-link of the system being proposed.

The DVR with PV power generation holds the load voltage, DC-link voltage, and grid voltage stable. Compared to existing structures, the new design offers the following advantages. The DC-link is integrated with the load point and dynamic voltage restorer. To stabilize the DC-link voltage, the DC-link is integrated with the PV power generation. The PV system with battery supports the DVR and the load point via the DC-link for the load profile maintenance. DVR with the PV power generating system will provide the required active and reactive energy to the electric power distribution system. The DVR recovers the device voltage that is connected through the line in series. The DC power or external battery-powered DVR offers an efficient injection of the unbalanced voltage but the cost is high. The DVR should be supplied with sufficient DC-link power, to protect the sensitive load, rather than with a separate source via a voltage source converter. The DC-link of DVR in this setup again relies upon the voltage of the power supply and cannot be stable to compensate for the line voltage. DVR may not protect the sensitive load under abnormal conditions. DC-link line interference can be prevented by integrating renewable energy with an energy storage system. Solar PV power with battery is used to supply the required DC-link power and to supply a continuous load power with power quality enhancement.

In this article, the second section describes the ZSI-based DVR topology and DC-DC converter with solar photovoltaic. The next section deals with the control scheme for ZSI-based solar PV interconnected DVR. The final section discusses the simulation and experimental results of the proposed ZSI-based solar PV powered DVR.

2. Proposed ZSI-based DVR topology

DVR is a power electronic circuitry that is used to transform voltages from the DC battery/PV system to the AC system as a voltage source inverter (VSI). The boost transformer unit transmits the voltage to the distribution system from the DVR for the compensation of voltage based disturbances.

The primary winding is connected to the power system in series and the secondary winding with the DVR is connected. The harmonic filter consists of an LC circuit to minimize the waveform harmonic distortion generated by VSI. Figure 1 displays the proposed solar PV power generation with a dynamic voltage restorer. The solar PV system's main module comprises solar PV with boost converters, ZSI converter, battery storage unit with DC-DC converter, AC loads, and the power grid. The utility grid is fed to the load through the DVR. The DC link is interfaced with solar photovoltaic with DC-DC converter and battery storage unit. The critical loads are protected by DVR and by the solar PV generation connected with the grid. The voltage

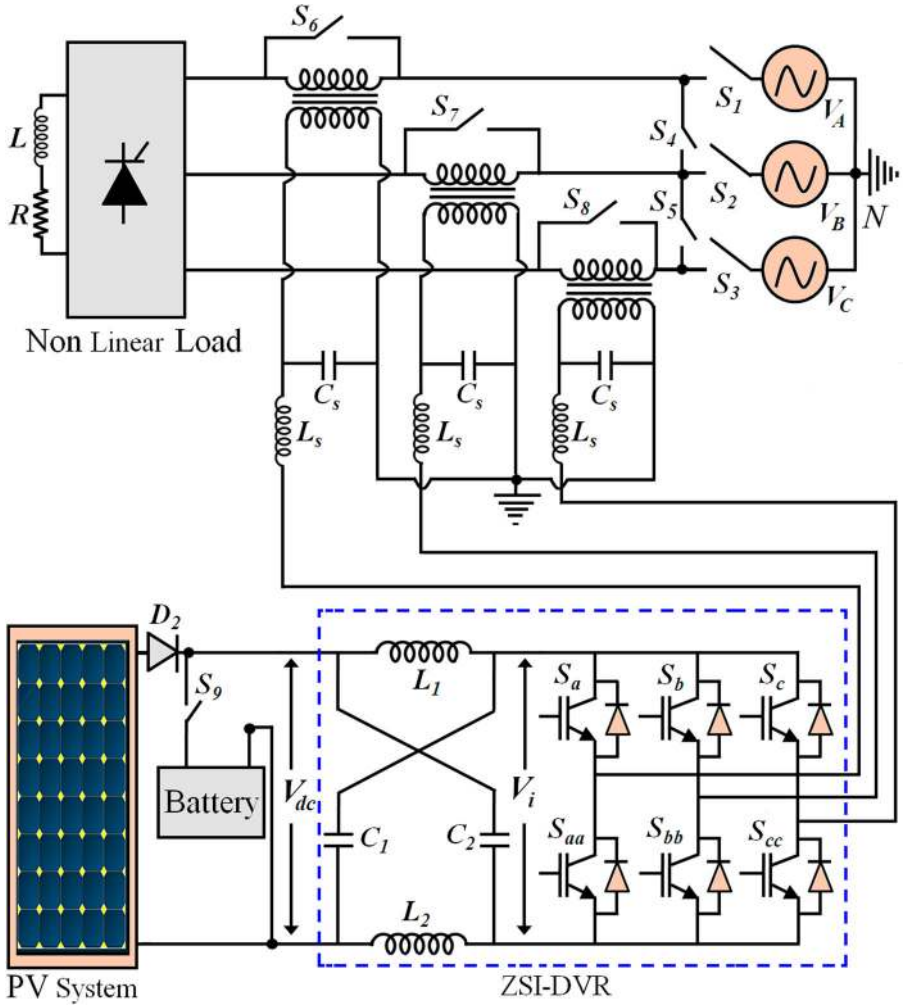

Figure 1. Proposed solar PV power generation with a ZSI-based dynamic voltage restorer.

is also regulated at the DC-link and the power transmission efficiency in the distribution line is increased. The battery storage system stabilizes power during the intermittent nature of the solar photovoltaic. The solar photovoltaic system with the battery supports the DC-link when the maximum energy is needed in the daytime.

2.1. Solar photovoltaic with DC-DC converter

Solar energy is abundant, tremendously accessible in nature and less inertia. The solar PV system is based on the photoelectric effect theory, which transforms solar energy into electricity. Solar PV power is fed to the DC-link by boosting the DC voltage through the

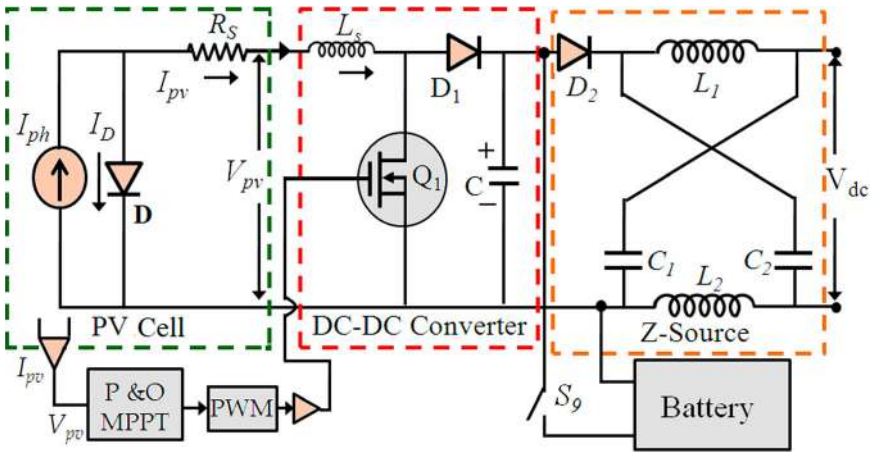

Figure 2. Solar PV with a Z-source network.

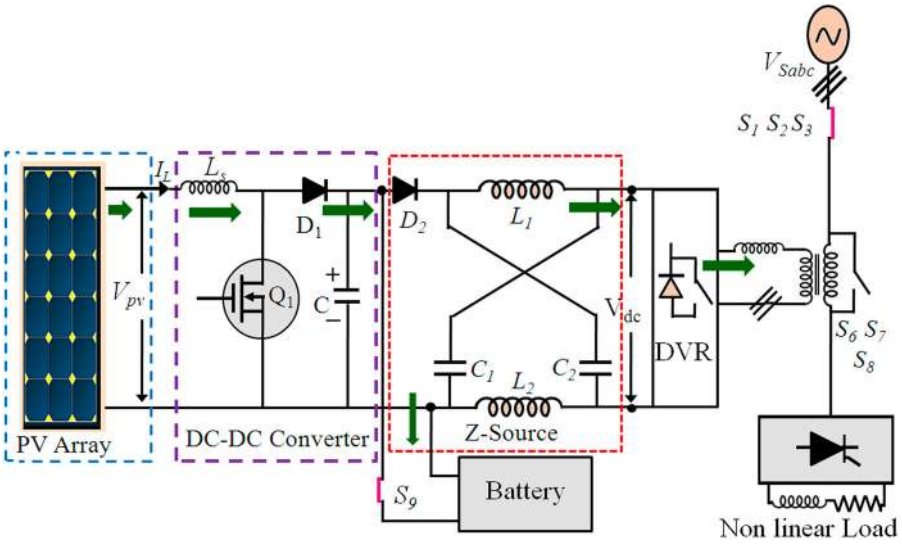

Figure 3. Mode 1 operation schematic circuit diagram.

DC-DC converter for the constant voltage of the DC-link. Figure 2 shows solar PV with a Z-source network structure. A single diode model is the best approach: a current source, as seen in Figure 2, in parallel with a diode, where the current source's output is directly proportional to light on the PV cell. This model includes only three parameters, namely short circuit current (I_{sc}), open-circuit voltage (I_{oc}) and diode ideality factor, which can completely define the I–V curve. The incorporation of series resistance allows an enhancement of the single diode model. This model is generally referred to as the R_s model. The R_s model is by far the most common in PV system simulation because of its simplicity and computational efficiency. The comparative findings lead to the assessment of the best single-diode photovoltaic model design that is more suited for different implementations of the power systems, regardless of the varying atmospheric conditions at various times of the day. The solar PV array is modelled according to the fundamental equations [18].

$$V_{pv} = \frac{nKT}{q \ln\left((I_{sc}/I_{pv}) + 1\right)} \tag{1}$$

$$I_{pv} = I_{ph} - I_D \times \left[\exp\left(\frac{q(V_{pv} + I_{ph}R_s)}{N_s K T_n} - 1\right)\right] - \frac{(V_{pv} + I_{ph}R_s)}{R_s} \tag{2}$$

Let I_{Ph} represents photocurrent (A), I_{PV} and V_{PV} represent the solar current (A) and PV voltage (V), K represents the Boltzmann constant, I_D represents the diode saturation current (A), T_n represents the PV cell reference temperature (^{O}C), n represents the ideality factor of the diode, Ns represents the number of series-connected PV cells, q is electron charge (coulombs) and R_S is the series resistance (Ω).

2.2. Operating modes of solar PV supported ZSI-DVR

The ZSI-DVR system supported by PV and battery worked in three possible operating modes [19]. Because of the multi-mode capability of the topology proposed, it manages the various situations effectively (voltage interruption, night time, maintenance, etc.) and provides the continuous clean power for the load.

2.2.1. Mode: 1

Due to the availability of solar irradiation, the output power of the PV generating system is high. The voltage sag/swell and reactive power in the grid supply is compensated by the PV-DVR system in this operating mode. Simultaneously, the excess PV power is provided to meet the demand for load and charges the battery storage unit. Mode 1 operation schematic circuit diagram is shown in Figure 3.

2.2.2. Mode: 2

The grid is disconnected from the load by semiconductor switches S_1, S_2, and S_3 during the voltage interruption period. The PV system /battery is responsible for meeting a critical load requirement during this period. Mode 2 operation schematic circuit diagram is shown in Figure 4.

2.2.3. Mode: 3

The PV generation system is shut down for maintenance purposes during the maintenance period. PV-DVR is separated using a bypass semiconductor switches S_6, S_7, and S_8 from series injection transformers. Mode 3 operation schematic circuit diagram is shown in Figure 5. The status of the switches for the different operating modes of PV supported ZSI-DVR is shown in Table 1.

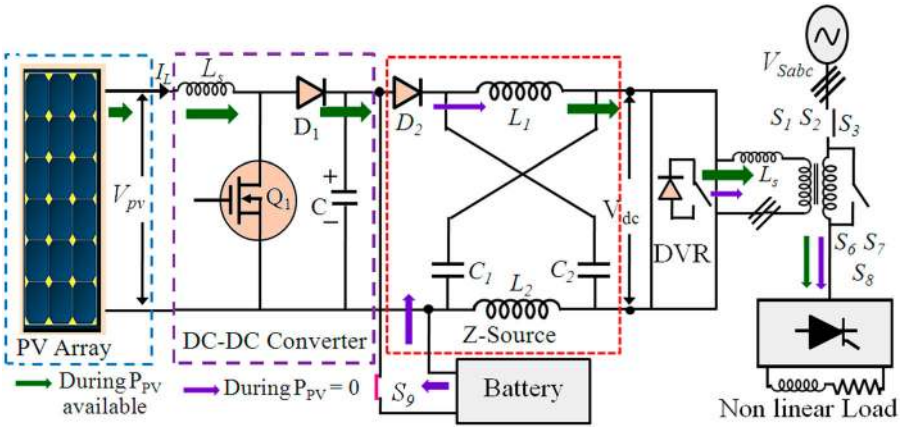

Figure 4. Mode 2 operation schematic circuit diagram.

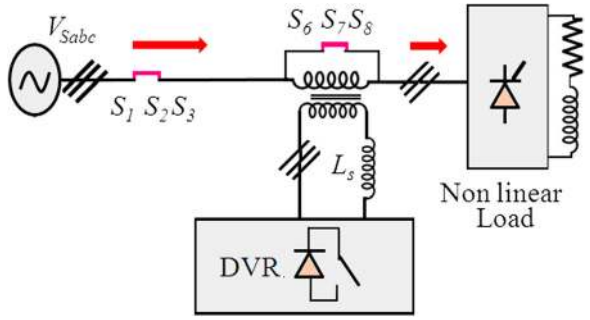

Figure 5. Mode 3 operation schematic circuit diagram.

3. Control scheme of solar PV interconnected ZSI-based DVR

The control algorithm based on U-SOGI is shown in Figure 6 is used to filter off harmonic load current components and extract the basic component for DVR switching pulse generation. This algorithm extracts both in-phase and quadrature elements from sensed load currents and measures the harmonics of load currents. For dynamic changes, a damping factor has been added to rapidly damp oscillations. Sensitive load currents are also used in their extraction of basic power components.

The Quadrature Signal Generator (QSG) is used as a building block for the SOGI algorithm as well as for a feedback circuit to find and transmit the load current to the controller in an error-less phase and frequency [14]. An additional integrator is included in the QSG block in conjunction with traditional SOGI to dampen the constant DC offset portion from the load current.

The transfer function of the feedback loop for the traditional SOGI algorithm as the orthogonal signal generator (OSG) is derived by the following equation:

$$f_{SOGI}(S) = \frac{\omega s}{s^2 + 2\omega s + \omega^2} \tag{3}$$

To decrease the error between sensed and real value, a damping factor is added to this OSG block. To reduce system oscillations during dynamic load changes, the damping factor is applied. A higher value increases the system's oscillation [20,21].

For U-SOGI algorithm, modified from a traditional SOGI algorithm, the OSG block transfer function is indicated as

$$f_{USOGI}(S) = \frac{\omega(s + \rho)}{(s + \rho)^2 + \omega^2} \tag{4}$$

The traditional SOGI algorithm cannot eliminate DC offset and inter harmonic elements present in the input load currents. For the DC offset attenuation, a low-pass filter can be inserted into the system, but it again disrupts traditional SOGI algorithm filter efficiency [22]. In the derived essential active and reactive amplitude, the traditional SOGI has more oscillations than the U-SOGI and DC offsets. In comparison, there is no DC offset component and no oscillations in the fundamental amplitude obtained using the USOGI algorithm.

The component of I_{loss} is a function of DC-link voltages. FLC based terminal voltage controller is employed to the I_{qq} component. The reference source current is determined by the summing I_{loss} component, I_{qq} component, an average of all load currents in phases and the average of all load currents in quadrature components [23,24]. The active in-phase voltage templates are

Table 1. Switching status for the different operating modes of PV supported ZSI-DVR.

		Status of the switches								
Modes of operation		S_1	S_2	S_3	S_4	S_5	S_6	S_7	S_8	S_9
Compensating Period	Mode 1	ON	ON	ON	OFF	OFF	OFF	OFF	OFF	ON
Voltage Interruption Period	Mode 2	OFF	OFF	OFF	ON	ON	OFF	OFF	OFF	OFF
Maintenance Period	Mode 3	ON	ON	ON	OFF	OFF	ON	ON	ON	OFF

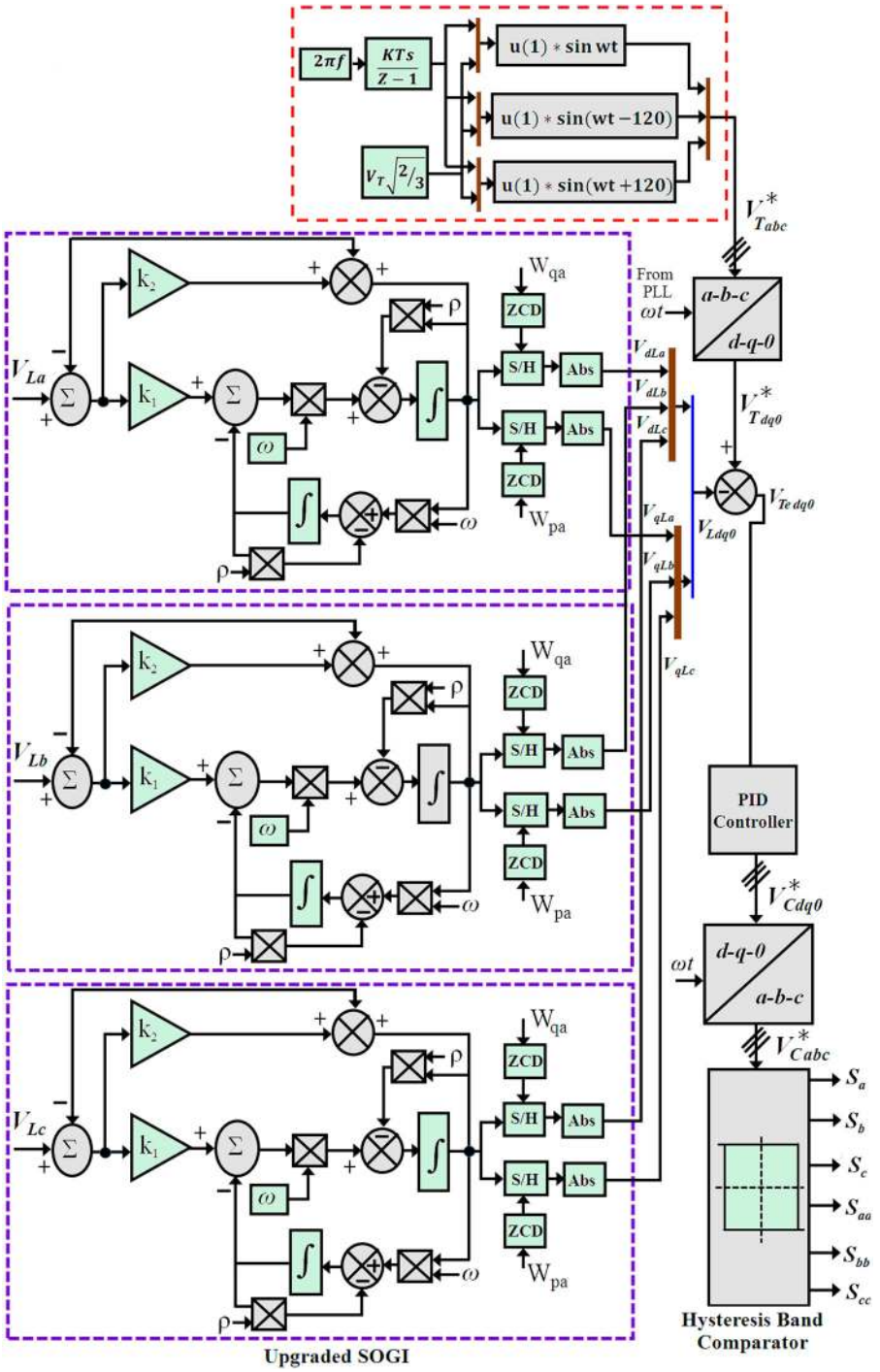

Figure 6. Control algorithm based on upgraded-SOGI.

formed as follows by line voltages.

$$\begin{bmatrix} w_{pa} \\ w_{pb} \\ w_{pc} \end{bmatrix} = \frac{1}{3V_T} \begin{bmatrix} 10-1 \\ -110 \\ 1-10 \end{bmatrix} \begin{bmatrix} V_{sab} \\ V_{sbc} \\ V_{sca} \end{bmatrix} \tag{5}$$

Let V_{sab}, V_{sbc} and V_{sac} are estimated phase voltages from line voltages and w_{pa}, w_{pb} and w_{pc} are active in-phase voltage templates.

$$\begin{bmatrix} V_{sa} \\ V_{sb} \\ V_{sc} \end{bmatrix} = \frac{1}{3} \begin{bmatrix} 21 \\ -11 \\ -1-2 \end{bmatrix} \begin{bmatrix} V_{sab} \\ V_{sbc} \end{bmatrix} \tag{6}$$

The quadrature unit templates of the phase voltage components (w_{qa}, w_{qb} and w_{qc}) are determined by the following equation:

$$\begin{bmatrix} w_{qa} \\ w_{qb} \\ w_{qc} \end{bmatrix} = \frac{1}{2\sqrt{3}} \begin{bmatrix} 0 & -2 & 2 \\ -3 & 1 & -1 \\ 3 & 1 & -1 \end{bmatrix} \begin{bmatrix} w_{pa} \\ w_{pb} \\ w_{pc} \end{bmatrix} \tag{7}$$

The voltage level of the terminal is determined as

$$V_T = \sqrt{2/3}\sqrt{V_{sa}^2 + V_{sb}^2 + V_{sc}^2} \tag{8}$$

The three-phase reference terminal voltage is estimated by the following equation:

$$\begin{bmatrix} V_{Ta}^* \\ V_{Tb}^* \\ V_{Tc}^* \end{bmatrix} = V_{T-\max} \begin{bmatrix} \sin \omega t \\ \sin(\omega t - 120) \\ \sin(\omega t + 120) \end{bmatrix} \quad (9)$$

It is then transformed from *abc* – *dq*0 components using *abc* – *dq*0 transformation unit. The *dq*0 transformation of the reference terminal voltage is derived as

$$\begin{bmatrix} V_{Tda}^* \\ V_{Tqb}^* \\ V_{T0c}^* \end{bmatrix} = \frac{2}{3} \begin{bmatrix} \cos(\omega t) & \cos(\omega t - 120) & \cos(\omega t + 120) \\ -\sin(\omega t) & -\sin(\omega t - 120) & -\sin(\omega t + 120) \\ \frac{1}{2} & \frac{1}{2} & \frac{1}{2} \end{bmatrix} \times \begin{bmatrix} V_{Ta}^* \\ V_{Tb}^* \\ V_{Tc}^* \end{bmatrix} \quad (10)$$

The error signal V_{Tedq0} has been determined by comparison of the reference voltage and load voltage *dq*0 component.

$$|V_{Tedq0}| = \sqrt{(V_{Td}^* - V_{Ld})^2 + (V_{Tq}^* - V_{Lq})^2 + (V_{T0}^* - V_{L0})^2} \quad (11)$$

An error-driven Proportional Integer Derivative (PID) controller is used to control the proposed PV-DVR function. The controller's role is to change the error signal on the power distribution grid to be minimized. The compensation signal is also taken from the PID controller in the *dq*0 reference frame for the generation of the gating pulses to DVR switches.

$$V_{Cdq0} = K_p V_{Tedq0} + K_i \int_0^1 V_{Tedq0} \mathrm{d}t + k_d \frac{\mathrm{d}V_{Tedq0}}{\mathrm{d}t} \quad (12)$$

where K_p, K_i, and K_d represent the proportional, integral and derivative gains of the PID controller respectively.

The PID controller output is returned to the three-phase *abc* reference frame to produce gating pulses on the DVR by using a hysteresis band comparator. The DVR compensation signals are generated and controlled by the feedback switching control by their actual values. The two control functions are configured, as they retain the grid voltage and load voltage, respectively under dynamic sources and load conditions.

$$\begin{bmatrix} V_{Ca}^* \\ V_{Cb}^* \\ V_{Cc}^* \end{bmatrix} = \begin{bmatrix} \sin(\omega t) & \cos(\omega t) & 1 \\ \sin(\omega t - \frac{2\pi}{3}) & \cos(\omega t - \frac{2\pi}{3}) & 1 \\ \sin(\omega t + \frac{2\pi}{3}) & \cos(\omega t + \frac{2\pi}{3}) & 1 \end{bmatrix} \times \begin{bmatrix} V_{Cd}^* \\ V_{Cq}^* \\ V_{C0}^* \end{bmatrix} \quad (13)$$

Let V_{Cd}^*, $V_{Cq}^*$and V_{C0}^* are estimated reference compensation voltage in *dq*0 reference frame and V_{Ca}^*, V_{Cb}^* and V_{Cc}^* are estimated reference compensation voltage in *abc* reference frame.

4. Results and discussions

MATLAB/Simulink has been used to create the SPV-DVR with the U-SOGI control scheme. To test the robustness of the control scheme, analyses of the balanced, unbalanced supply, dynamic unbalanced load, and various radiation systems for solar photovoltaic are conducted. A real-time experimental prototype built in the laboratory has been tested with the proposed control algorithm. Part of the hardware prototype image of ZSI-DVR is shown in Figure 7. The device is working at the reduction of the supply voltage through an autotransformer and is used as a non-linear load by the R-L diode bridge rectifier. Voltage sensors are used for detecting Point of Common Coupling (PCC) voltages, and solar PV array tension and Hall Effect current sensors are used to monitor grid currents and load currents. A Field-Programmable-Gate-Array (FPGA) controller is used to implement the proposed control algorithm. The required isolation between the ZSI-DVR and the FPGA signals can be provided by an

Figure 7. Hardware prototype image of ZSI-DVR.

Table 2. Parameters and ratings of the solar PV ZSI-DVR.

Label	Value	Unit	Description
V_s	230	V	Supply voltage
V_{DC}	600	V	DC-link voltage
L_f, C_f, R_f	5, 80, 1.5	mH, μF, Ω	Filter
f_s	10	kHz	Switching frequency
L	1	μH	Inductor (DC-DC converter)
C	200	μF	Capacitance (DC-DC converter)
f_{sd}	20	kHz	Switching frequency (DC-DC converter)
	60		No. of PV cells
P_{mp}	230	W	Maximum power
V_{mp}	35.5	V	Voltage at Max. power
I_{mp}	6.77	A	Current at Max. power
V_{oc}	43.6	V	Open-Circuit Voltage
I_{sc}	7.37	A	Short Circuit Current

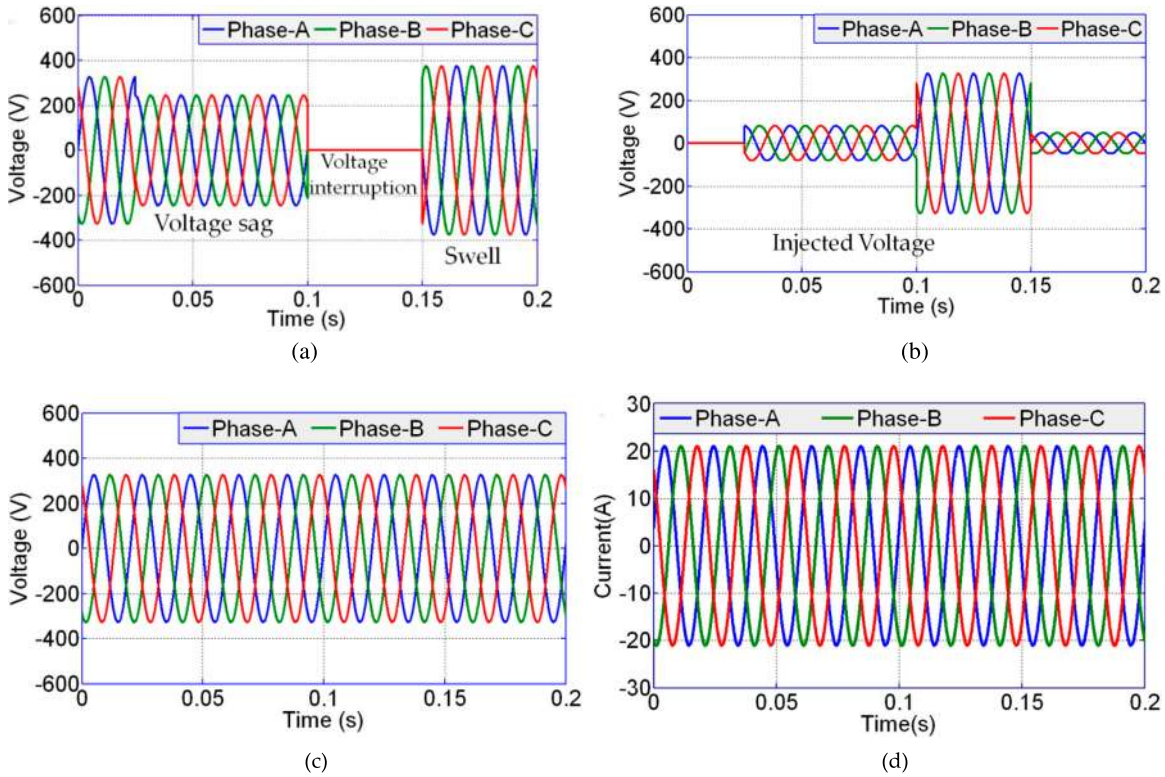

Figure 8. Simulation results under balanced voltages with balanced loads: (a) supply voltage with sag and interruption, (b) voltage injected by DVR, (c) DVR compensated Load voltage and (d) load current with SPV-DVR.

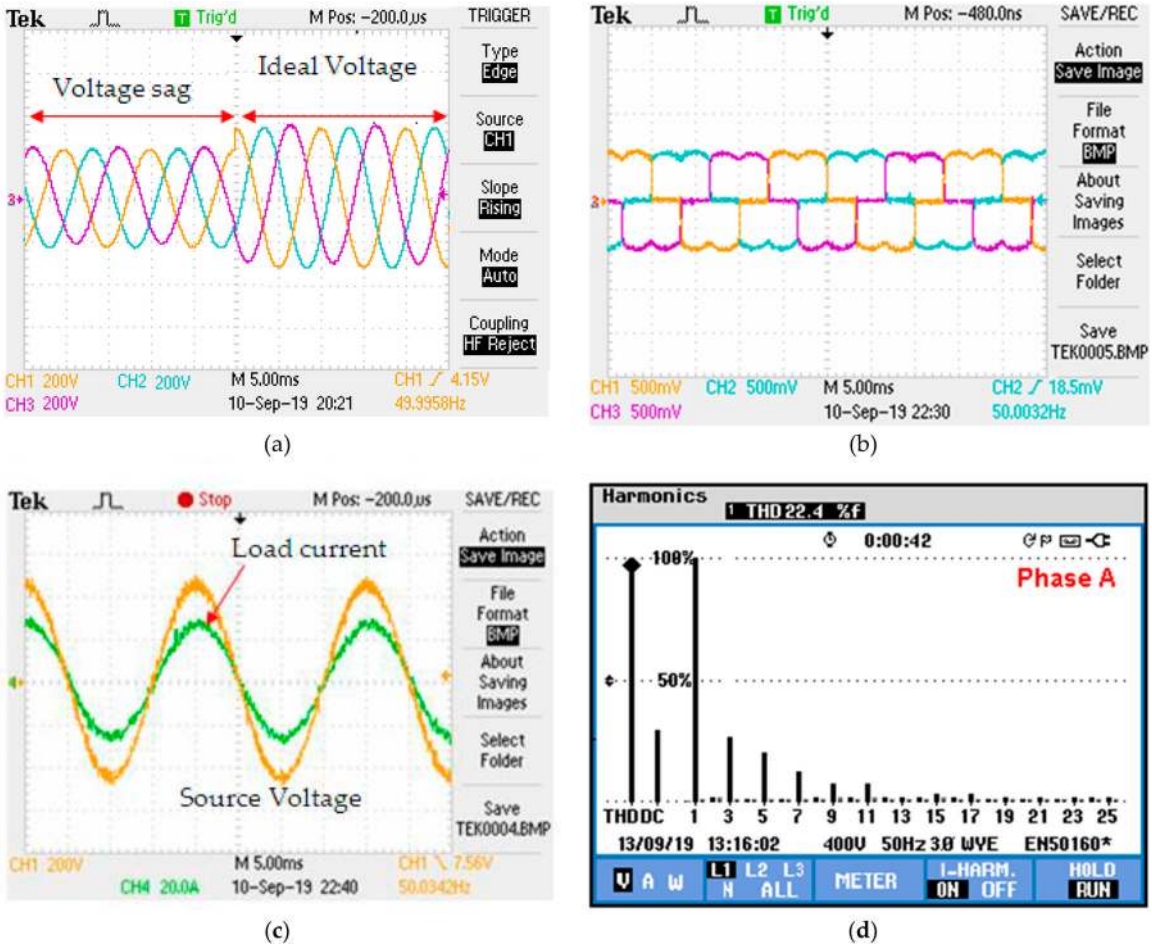

Figure 9. Experimental outcomes: (a) supply voltage with sag, (b) load current during case-1, (c) Load current and source voltage and (d) load voltage THD level for case-1 without SPV-DVR.

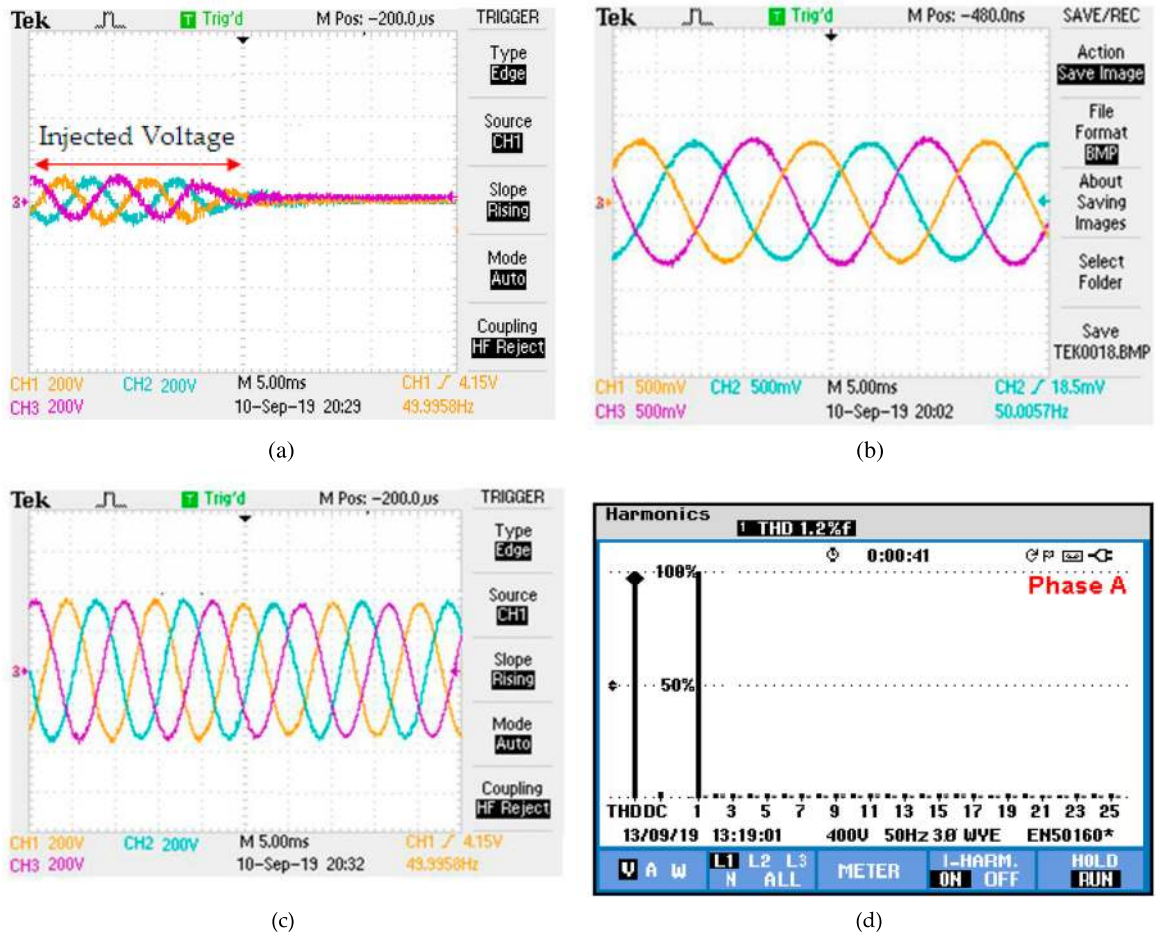

Figure 10. Experimental findings for SPV-DVR in balanced voltage and non-linear load: (a) voltage injected by DVR, (b) load current with SPV-DVR, (c) SPV-DVR compensated load voltage and (d) load voltage THD level for case-1 with SPV-DVR.

Figure 11. Experimental outcomes: (a) voltage of SPV array (b) SPV-DVR DC-link voltage.

Optocoupler. The detailed parameters and ratings of the proposed system are given in Table 2.

4.1. Case 1: balanced supply voltage with balanced non-linear load

Assessment of the control technique suggested under the specific load condition has been carried out. A resistive-inductive (R-L) load with a diode bridge rectifier is used as a non-linear load. Figure 8 illustrates the simulation findings for voltage and current compensation under balanced voltage supply and non-linear load.

An experimental investigation is performed with a balanced supply voltage and non-linear load for voltage and current compensation. Voltage and current

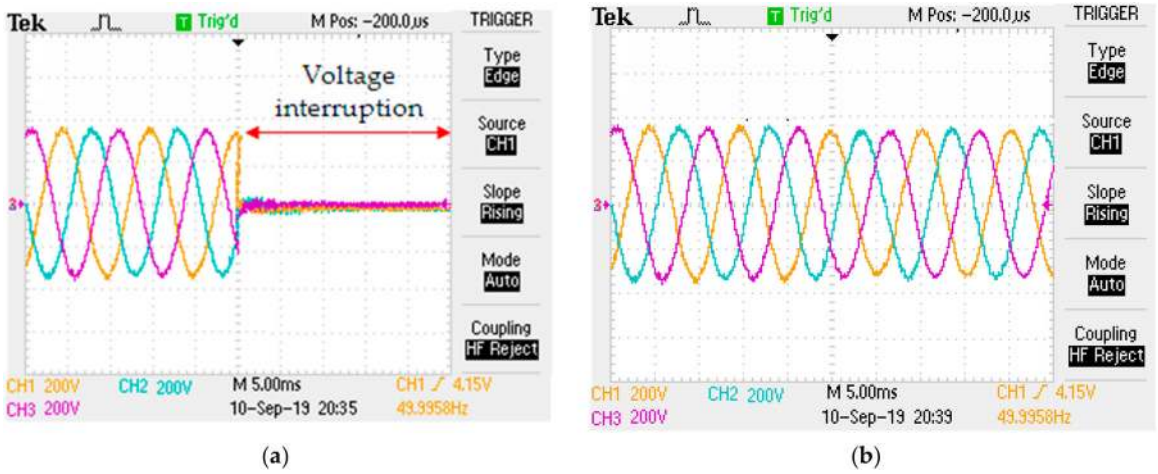

Figure 12. Experimental results despite the disturbance in voltage: (a) supply voltage with interruption and (b) SPV-DVR compensated load voltage.

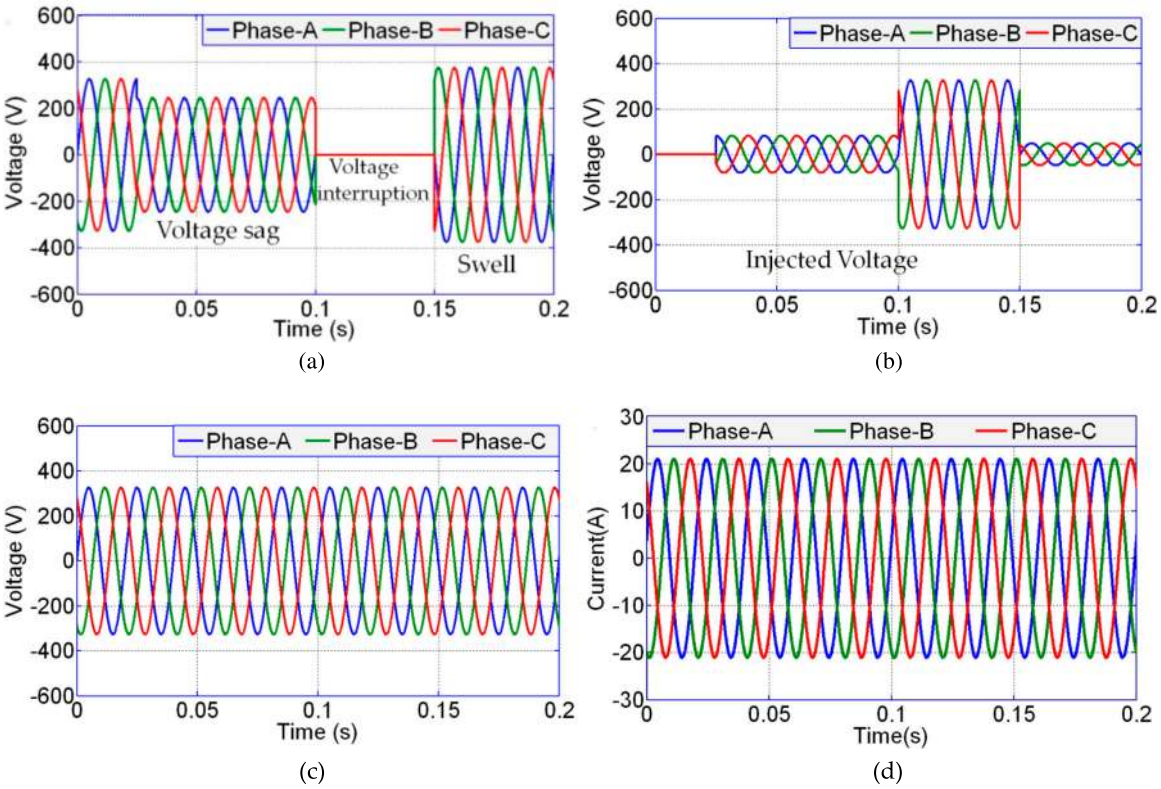

Figure 13. Simulation findings for SPV-DVR in balanced voltage and unbalanced non-linear load: (a) supply voltage with sag and interruption, (b) voltage injected by SPV-DVR, (c) SPV-DVR compensated load voltage and (d) load current with the SPV-DVR.

compensation outcomes of the experimental study under balanced voltage supply and non-linear load are shown in Figure 9.

The experimental findings for SPV-DVR in balanced voltage and non-linear load during the voltage compensation process are shown in Figure 10. The source current is maintained clean sinusoidal after compensation. The load voltage harmonic spectra with THD of 1.2%, whereas without SPV-DVR the load voltage THD of 25.5%. The THD of the load voltage under load unbalancing is also within the IEEE-519 standard [25] as shown in Figure 10(d). PV supply is maintained constant throughout and thus a stable DC-link voltage can be observed from Figure 11.

Figure 12 shows the supply voltage and load voltage after compensation of voltage interruption. Figure 12(a) shows a similar set of waveforms with a sudden voltage reduction to zero. At that time, solar PV supported ZSI-DVR starts to compensate voltage interruption and injects the voltage to compensate for the voltage interruption present in the electric power distribution system.

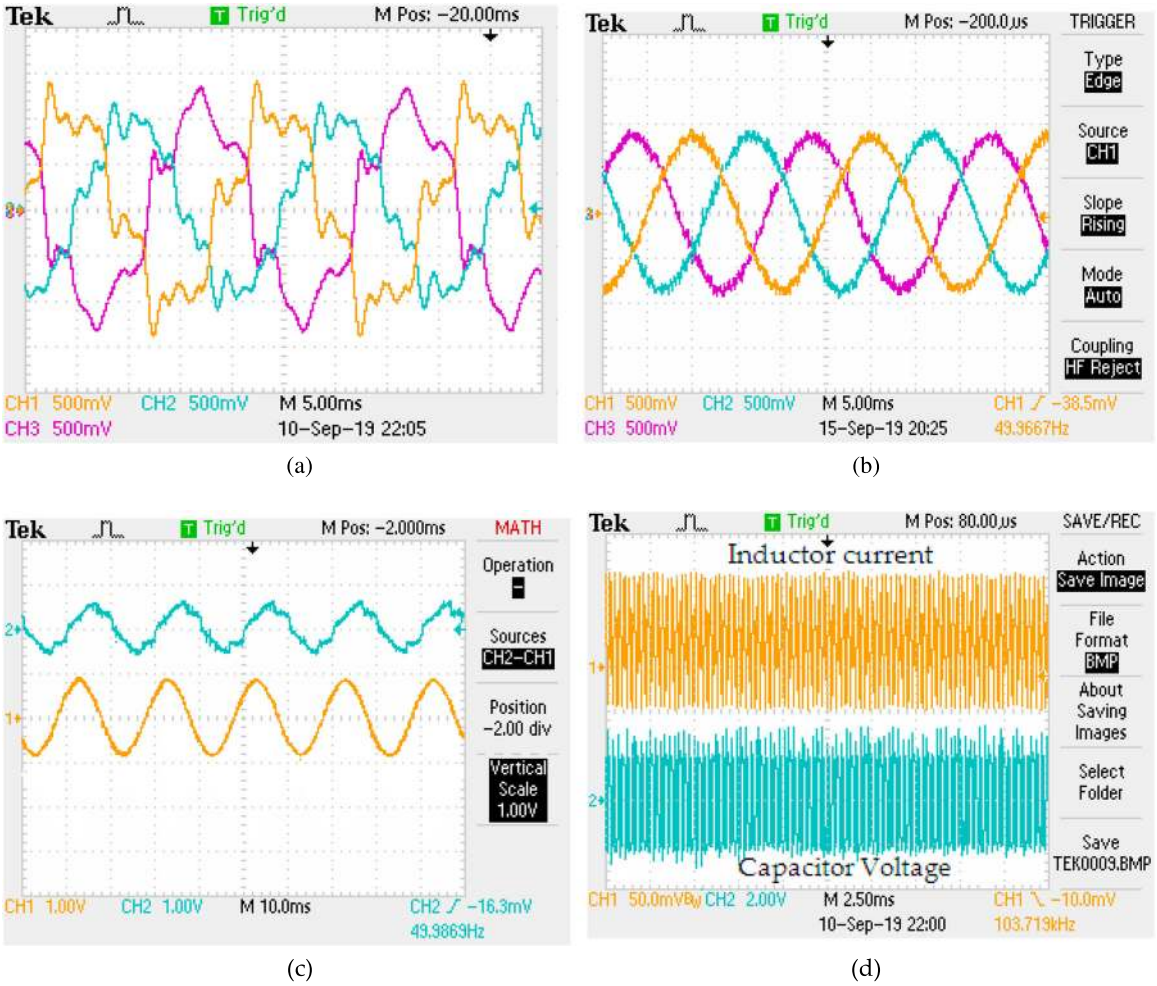

Figure 14. Experimental outcomes: (a) distorted unbalanced load current, (b) compensated source currents with ZSI-DVR (c) load and source current in phase-A and (d) filter inductor current and capacitor voltage.

4.2. Case 2: balanced supply voltage with unbalanced load

The desired performance of the PV-DVR system may poorly be affected due to unbalancing the load current. To verify the efficiency of the proposed control method under such conditions, simulation and experimentations have been carried out. The U-SOGI based PV-DVR behaviour under balanced supply voltage and unbalanced non-linear loaded conditions are shown in Figures 13 and 14. Figure 13 shows the source voltage, injected voltage, compensated load voltage and load current. At the beginning of steady-state voltage compensation analysis, the rated voltage (230V in RMS) is applied after that voltage sag and voltage interruption is applied. The solar PV ZSI-DVR identifies the voltage sag and voltage interruption and injects an appropriate compensating voltage in series with the supply voltage to eliminate the voltage sag.

Figure 14 shows the experimental outcomes of load current, compensated source current and load and source current in the phase-A and inductor current and capacitor voltage of the LC filter.

Due to the connection of non-linear and unbalanced load in the system, the load currents are distorted by the harmonics. After connecting the solar PV supported ZSI-DVR, the source current waveforms are compensated by injecting an appropriate compensation current. The experimental outcomes for SPV-DVR in balanced voltage and unbalanced non-linear load during voltage compensation progression are shown in Figure 15. The PV array output voltage and the voltage across the DC – link of ZSI-DVR is shown in Figures 16 and 17. The PV array output voltage magnitude is stepping up into 600 V by using the Z-source network.

Figure 18 shows the dynamic characteristics of the DC-link voltage control of the solar PV interfaced ZSI-DVR. The PV power generating system is maintained a stable DC-link voltage of the DVR can be observed from Figure 18(a, b).

The THD level of the load voltage without solar PV supported ZSI-DVR is 24.2(%) in phase-A and THD level of the load voltage with solar PV supported ZSI-DVR is 1.2(%) in phase-A shown in Figure 19. FFT analysis of source and load current has been carried out

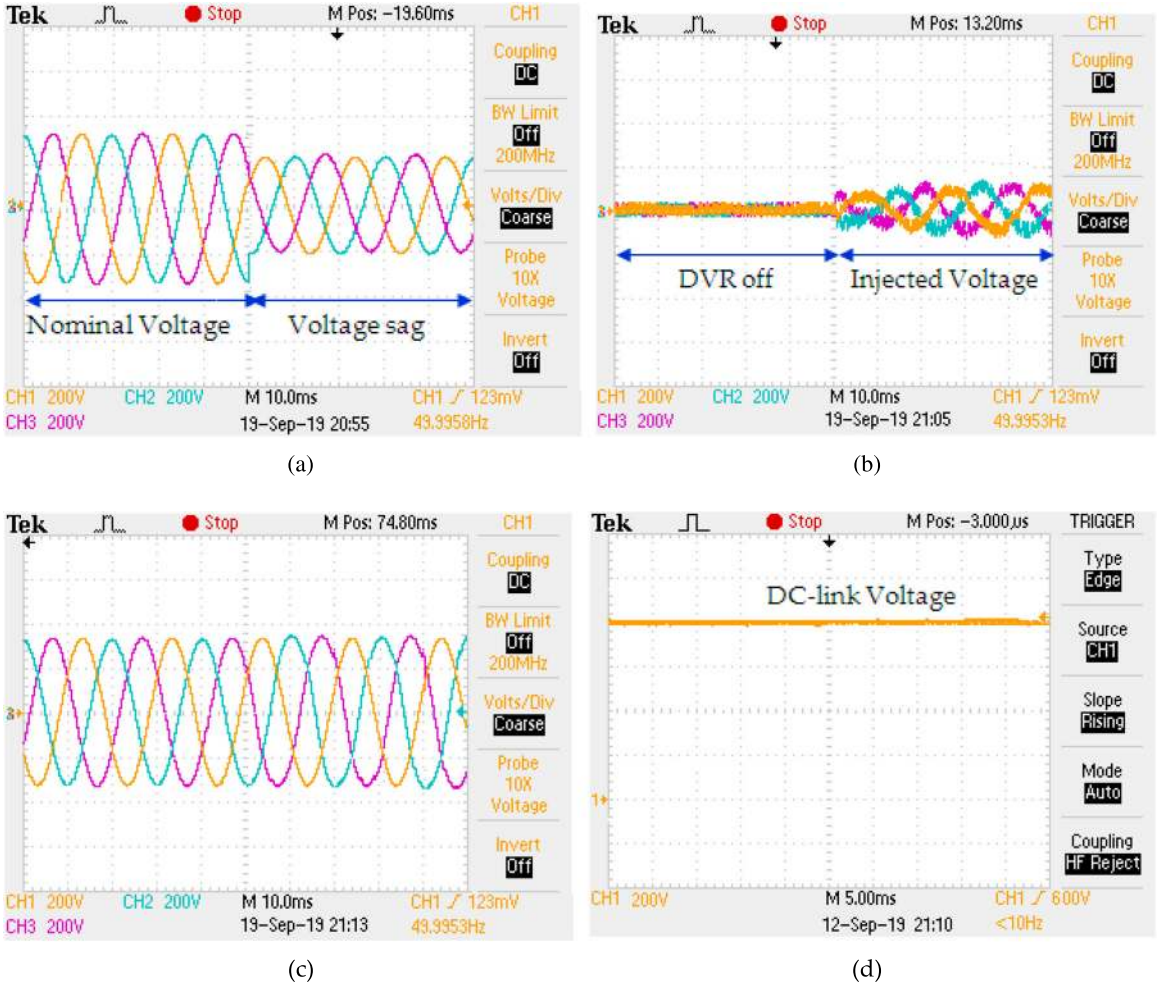

Figure 15. Experimental outcomes for SPV-DVR in balanced voltage and unbalanced non-linear load: (a) supply voltage with sag, (b) SPV-DVR injected voltage, (c) SPV-DVR compensated load voltage and (d) SPV-DVR DC-link voltage.

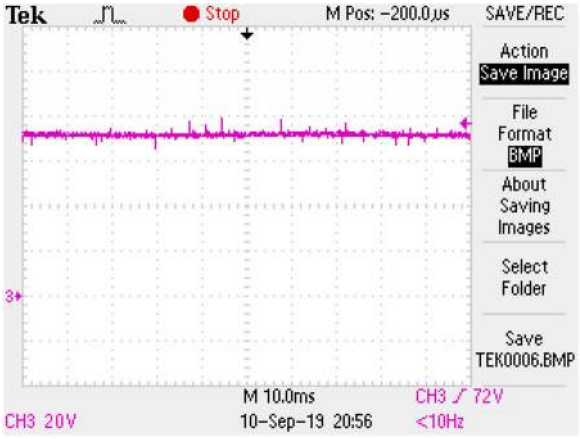

Figure 16. PV array output voltage.

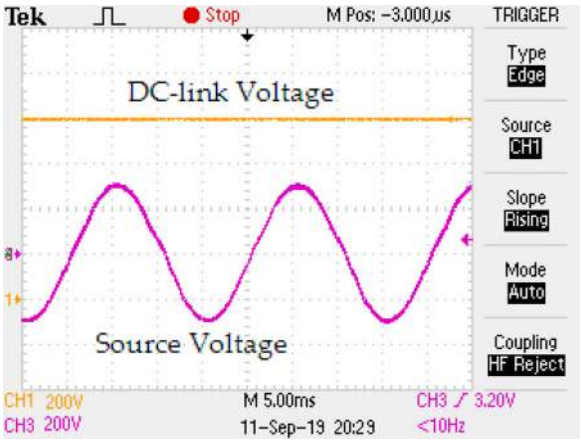

Figure 17. SPV-DVR DC-link voltage and source voltage.

for the stable source voltage and unstable load current condition. The THD level of the load voltage without solar PV supported ZSI-DVR is 24.2%, 23.7%, and 24.10% and with solar PV supported ZSI-DVR THD level of the load voltage is 1.2%, 1.3%, and 1.2%.

4.3. Case 3: unbalanced supply voltage with dynamic load condition

The desired performance of the PV-DVR system may poorly be affected due to unbalancing in the grid voltage. To verify the effectiveness of the proposed

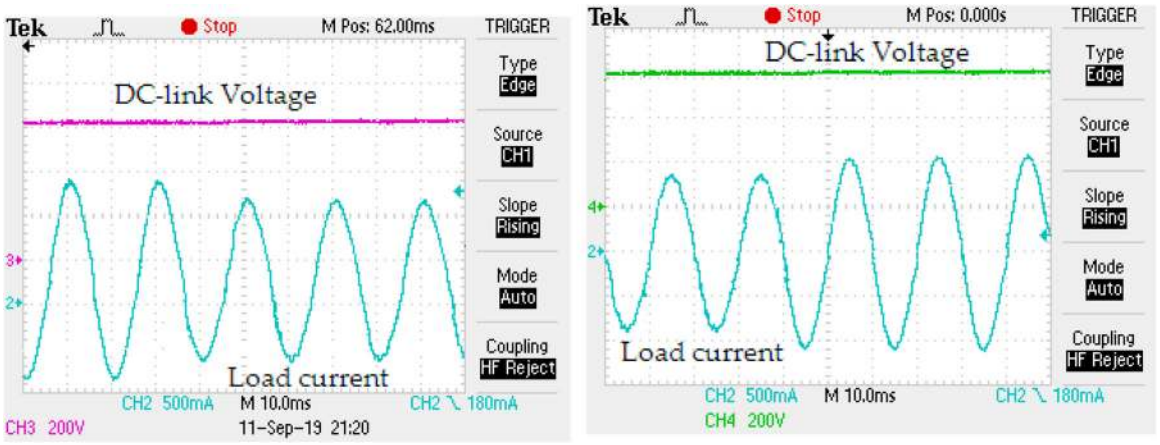

(a) (b)

Figure 18. Dynamic performance of DC-link voltage control: (a) during load current decrease and (b) during load current increase.

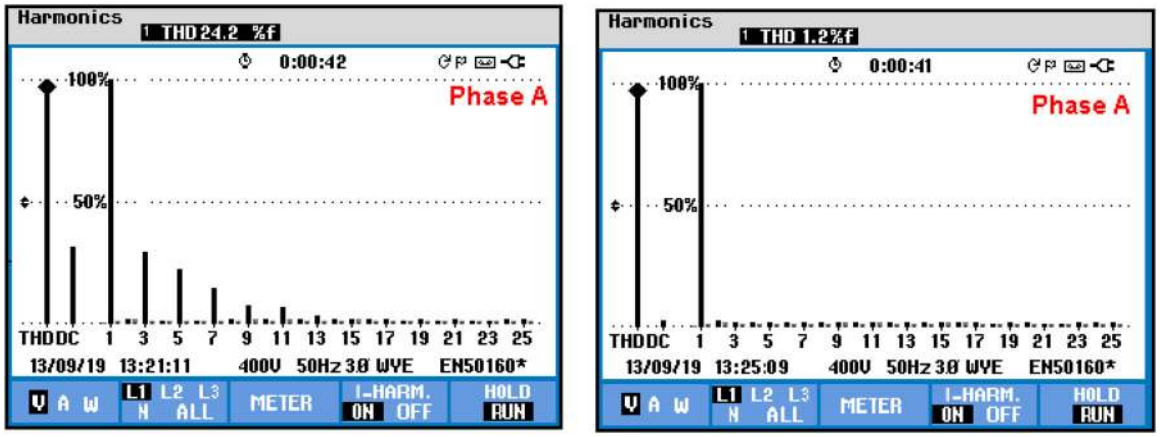

(a) (b)

Figure 19. THD level of the load voltages: (a)without solar PV supported ZSI-DVR (b) with solar PV supported ZSI-DVR.

control method under such conditions, experimentations have been carried out. The U-SOGI based PV-DVR behaviour under unbalanced supply voltage and dynamic non-linear loaded conditions are shown in Figures 20 and 21. The outcomes of digital simulation for voltage and current compensation under unbalanced supply voltage and non-linear load are shown in Figure 20.

Figure 21 shows the digital simulation results of PV array output voltage, DC-link voltage of the ZSI-DVR, THD level of load voltage without ZSI-DVR and THD level of load voltage with ZSI-DVR under the conditions of unbalanced voltages and load currents.

Experimental test results of unbalanced distorted load currents, unbalanced source voltages and harmonic distortions in a load voltage before connecting the solar PV ZSI-DVR under the unbalanced supply voltage and load conditions are shown in Figure 22.

Figure 23 shows the series transformer injected voltage, load voltage with the SPV-DVR, load current with solar PV ZSI-DVR and load voltage THD level in phase-A for case-3 with solar PV ZSI-DVR.

THD (%) level of the load voltage without the use of SPV-DVR is 23.2, 24.6, and 24.1; they are diminished to 1.3, 1.2, and 1.3 consistently with the use of SPV-DVR. The output of solar PV-DVR is tested with regard to the THD level of load voltage. Load voltages THD level with the use of solar PV ZSI-DVR and without the use of solar PV ZSI-DVR is shown Table 3. The THD measurement thresholds are very small and suitable for grid-connected applications based on the simulation and experiment outcomes. The performance of the solar PV supported ZSI-DVR is examined in terms of THD of load voltage. From the results of both simulation and experimental study, it is noticeable that load voltage THD is found to be well within 5% of the boundary indicated by IEEE Std. 519–1992 [25].

For non-linear load conditions, the voltage harmonics THD level is very less in the proposed method, approximately 1.2% compared to the existing methods

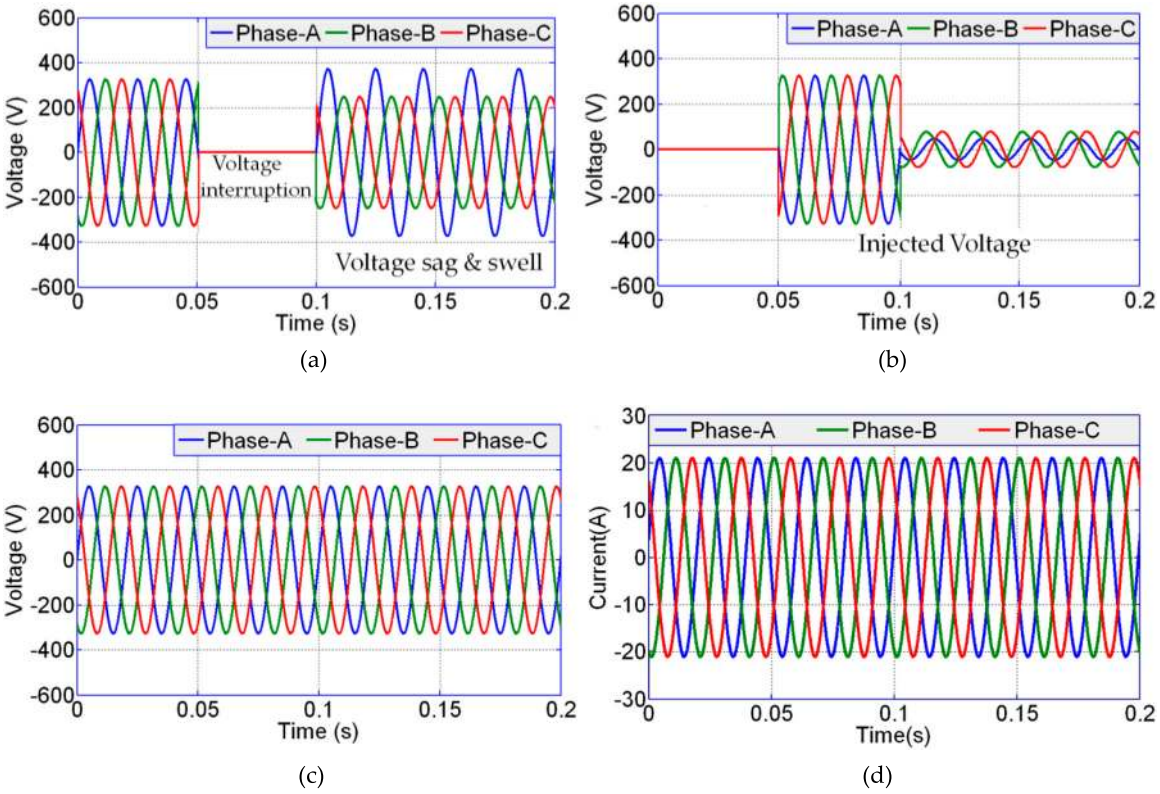

Figure 20. Outcomes of digital simulation: (a) supply voltage with sag and interruption, (b) SPV-DVR injected voltage, (c) load voltage with the SPV-DVR and (d) load current with solar PV ZSI-DVR.

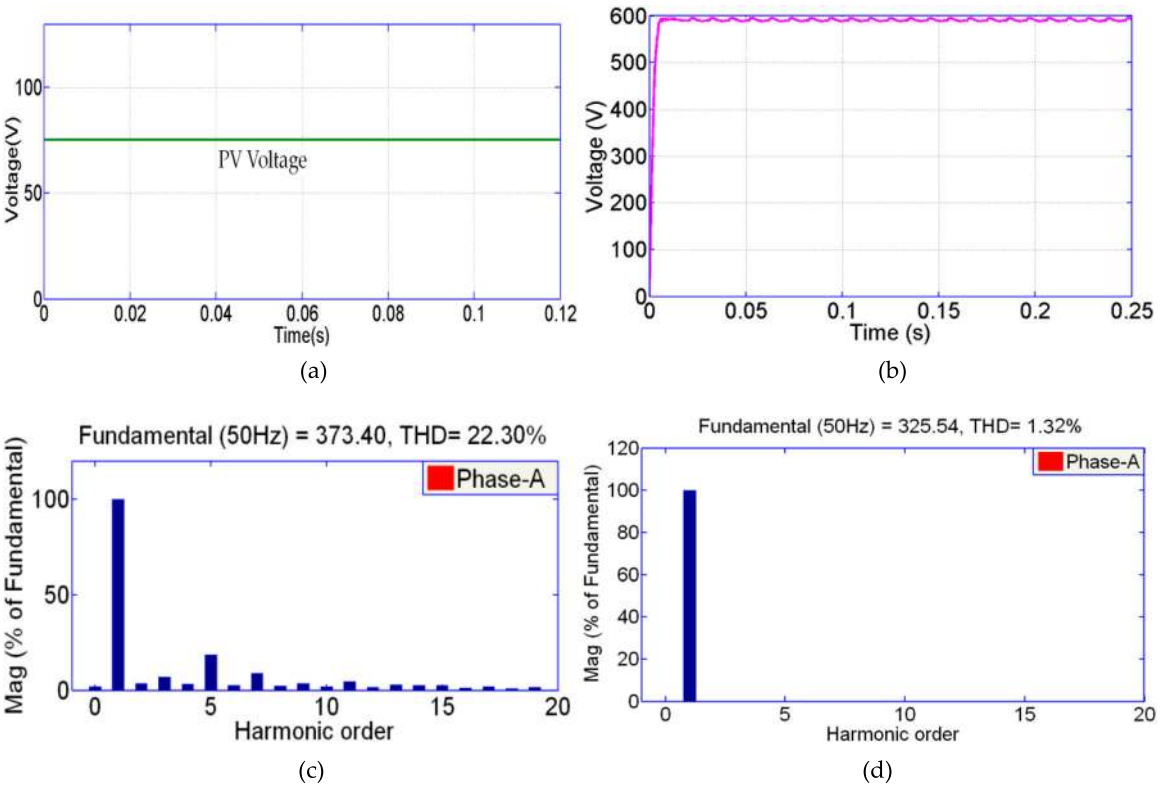

Figure 21. Digital simulation results: (a) PV array output voltage, (b) DC-link voltage of ZSI-DVR, (c) Load voltage THD level for case-3 without SPV-DVR and (d) load voltage THD level for case-3 with the SPV-DVR.

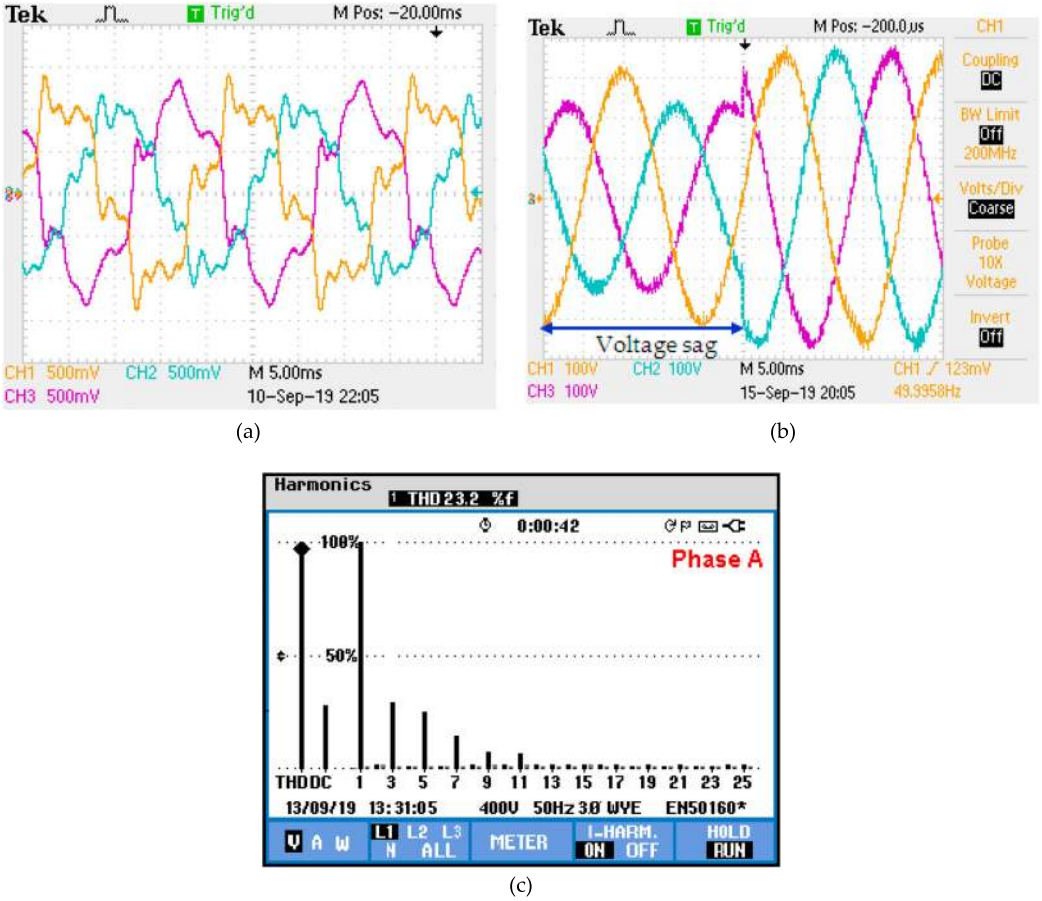

Figure 22. Experimental outcomes for case-3: (a) load currents without SPV-DVR, (b) supply voltage with unbalanced sag and (c) load voltage THD level for case-3 without SPV-DVR.

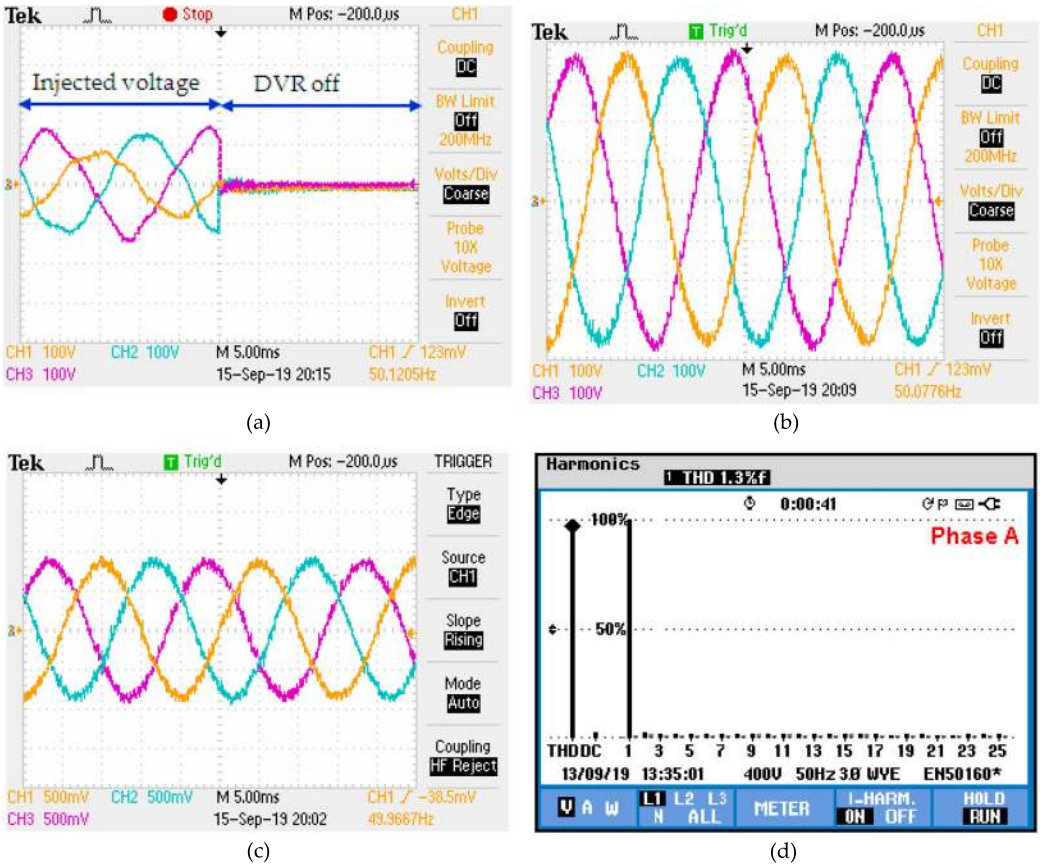

Figure 23. Experimental test results: (a) series transformer injected voltage, (b) load voltage with solar PV ZSI-DVR, (c) Load current with solar PV ZSI-DVR and (d) load voltage THD level in phase-A for case-3 with the SPV-DVR.

Table 3. Load voltages THD level with the use of solar PV ZSI-DVR and without the use of solar PV ZSI-DVR.

	Outcomes of Simulation						Outcomes of Experimentation					
	1		2		3		1		2		3	
Case Phase	Without Compensator Voltage THD (%)	Solar PV- ZSI-DVR Voltage THD (%)	Without Compensator Voltage THD (%)	Solar PV- ZSI-DVR Voltage THD (%)	Without Compensator Voltage THD (%)	Solar PV- ZSI-DVR Voltage THD (%)	Without Compensator Voltage THD (%)	Solar PV- ZSI-DVR Voltage THD (%)	Without Compensator Voltage THD (%)	Solar PV- ZSI-DVR Voltage THD (%)	Without Compensator Voltage THD (%)	Solar PV- ZSI-DVR Voltage THD (%)
A	22.4	1.2	24.2	1.2	23.2	1.3	22.50	1.31	23.10	1.30	22.30	1.32
B	23.0	1.1	23.7	1.3	24.6	1.2	23.45	1.28	23.15	1.25	23.60	1.25
C	23.2	1.1	24.1	1.2	24.1	1.3	24.10	1.32	23.50	1.28	24.50	1.23

with a load voltage THD of 4.54% as presented by Pradhan and Mishra (17) [17].

5. Conclusion

In this paper, the benefits of distributed generation integration in a distribution network with an emphasis on power quality improvement have been addressed by employing the proposed U-SOGI based PV-DVR system. Voltage sag/swell and harmonic distortion has been considered in this paper as a power quality problem. Applying the proposed algorithm, the THD of source current has been maintained much below 5%, satisfying the IEEE-519 standard. The performance of the novel U-SOGI based control technique for voltage compensation reference signal generation is enhanced by proper tuning of parameters. A definitive analysis shows that maximum PV power is fed to the grid while effectively compensating the load harmonics using the proposed U-SOGI control technique. The experimental verification under different test cases has been presented to verify the validity of the proposed algorithm with a scaled-down laboratory prototype. Results obtained in all test cases have shown the improved performance of the system using the proposed control technique under steady-state as well as different dynamic conditions. The PV system has been ensured by using the reduced senor-based MPPT controller, which also helps to maintain the stable DC-link voltage in all conditions. The PV-DVR system suitably maintains the clean sinusoidal grid current under load and source unbalanced conditions as well as varying solar irradiation conditions.

Disclosure statement

No potential conflict of interest was reported by the author(s).

ORCID

T. Jayakumar http://orcid.org/0000-0001-8022-6162
Albert Alexander Stonier http://orcid.org/0000-0002-3572-2885

References

[1] Singh B, Chandra A, Al-Haddad K. Power quality: problems and mitigation techniques. Chichester: John Wiley & Sons Inc; 2015.
[2] Becirovic V, Helac V, Hanjalic S, et al. Power quality problems in autonomous photovoltaic system with energy storage. International Symposium on Power Electronics, Electrical Drives, Automation and Motion (SPEEDAM); 2018. p. 871–876. DOI:10.1109/SPEEDAM.2018.8445271.
[3] Hossain E, Tür MR, Padmanaban S, et al. Analysis and mitigation of power quality issues in distributed generation systems using custom power devices. IEEE Access 2018;6:16816–16833. DOI:10.1109/ACCESS.2018.2814981.

[4] El-Khattam W, Elnady M, Salama MMA. Distributed generation impact on the dynamic voltage restorer rating. IEEE PES Transm Distrib Conf Exposit. 2003;2: 595–599. DOI:10.1109/TDC.2003.1335343.
[5] Kanjiya P, Singh B, Chandra A, et al. SRF theory revisited to control self-supported dynamic voltage restorer (DVR) for unbalanced and nonlinear loads. IEEE Trans Ind Appl. 2013;49(5):2330–2340. DOI:10.1109/TIA.2013.2261273.
[6] Priyavarthini S, Kathiresan AC, Nagamani C, et al. PV-fed DVR for simultaneous real power injection and sag/swell mitigation in a wind farm. IET Power Electron. 2018;11(14):2385–2395. DOI:10.1049/iet-pel.2018.5123.
[7] M Vijayakumar, S Vijayan. Extended Reference Signal Generation Scheme for Integration of UPQC in Grid Connected PV System. Electr. Power Comp. Syst. 2015;43(8-10):914–927. DOI:10.1080/15325008.2015.1008708.
[8] Ogunboyo PT, Tiako R, Davidson IE. Effectiveness of dynamic voltage restorer for unbalance voltage mitigation and voltage profile improvement in secondary distribution system. Can J Electr Comput Eng. 2018; 41(2):105–115. DOI:10.1109/CJECE.2018.2858841.
[9] Ghosh A, Jindal AK, Joshi A. Design of a capacitor-supported dynamic voltage restorer (DVR) for unbalanced and distorted loads. IEEE Trans Power Deliv. 2004;19(1):405–413. DOI:10.1109/TPWRD.2003.820198.
[10] Li P, Xie L, Han J, et al. New Decentralized control scheme for a dynamic voltage restorer based on the elliptical trajectory compensation. IEEE Trans Ind Electron. 2017;64(8):6484–6495. DOI:10.1109/TIE.2017.2682785.
[11] Eddine KD, Mezouar A, Boumediene L, et al. A comprehensive review of LVRT capability and sliding mode control of grid-connected wind-turbine-driven doubly fed induction generator. Automatika. 2016;57(4):922–935. DOI:10.7305/automatika.2017.05.1813.
[12] Mallick N, Mukherjee V. Self-tuned fuzzy-proportional–integral compensated zero/minimum active power algorithm based dynamic voltage restorer. IET Gener Transm Distrib. 2018;12(11):2778–2787. DOI:10.1049/iet-gtd.2017.1170.
[13] Torres AP, Roncero-Sanchez P, Batlle VF. A two degrees of freedom resonant control scheme for voltage-sag compensation in dynamic voltage restorers. IEEE Trans Power Electron. 2018;33(6):4852–4867. DOI:10.1109/TPEL.2017.2727488.
[14] Khalghani MR, Shamsi-Nejad MA, Farshad M, et al. Modifying power quality's Indices of load by presenting an adaptive method based on Hebb Learning algorithm for controlling DVR. Automatika. 2014;55(2):153–161. DOI: 10.7305/automatika.2014.06.364.
[15] Nazarpour D, Farzinnia M, Nouhi H. Transformerless dynamic voltage restorer based on buck-boost converter. IET Power Electron. 2017;10(13):1767–1777. DOI:10.1049/iet-pel.2016.0441.
[16] Nourmohamadi H, Bektas SI, Hosseini SH, et al. A conventional dynamic voltage restorer with fault current limiting capability. Procedia Comput Sci. 2017;120:750–757. DOI:10.1016/j.procs.2017.11.305.
[17] Pradhan M, Mishra MK. Dual P-Q theory based energy-optimized dynamic voltage restorer for power quality improvement in a distribution system. IEEE Trans Ind Electron. 2019;66(4):2946–2955. DOI:10.1109/TIE.2018.2850009.
[18] Senguttuvan S, Vijayakumar M. Solar photovoltaic system interfaced shunt active power filter for enhancement of power quality in three-phase distribution system. J Circuits Syst Comput. 2018;27(11):1850166 (27 pages). DOI:10.1142/S0218126618501669.
[19] Vijayakumar M, Ramasamy M. Performance evaluation of UPQC for interconnecting photovoltaic systems to the electric grid. J Test Eval. 2016;44(4):1600–1616. DOI:10.1520/JTE20140474.
[20] Vijayakumar M, Vijayan S. Photovoltaic based three-phase four-wire series hybrid active power filter for power quality improvement. Indian J Eng Mater Sci. 2014;21(4):358–370. http://hdl.handle.net/123456789/29411.
[21] Gaolin W, Li D, Zhuomin L, et al. Enhanced position observer using second order generalized integrator for sensorless interior permanent magnet synchronous motor drives. IEEE Trans Energy Convers. 2014;29(2):486–495. DOI:10.1109/TEC.2014.2311098.
[22] Yang M, Tan T, Hu J. Simulation and experiment of algorithm and circuit design for UPQC. Automatika. 2019;60(4):480–490. DOI:10.1080/00051144.2019.1645401.
[23] Możdżyński K, Rafal K, Bobrowska-Rafal M. Application of the second order generalized integrator in digital control systems. Arch Electr Eng. 2014;63(3):423–437. DOI:10.2478/aee-2014-0031.
[24] Golestan S, Guerrero JM, Vasquez JC, et al. Modeling, tuning, and performance comparison of second order generalized integrator based FLLs. IEEE Trans Power Electron. 2018;33(12):10229–10239. DOI:10.1109/TPEL.2018.2808246.
[25] IEEE Std 519-2014. IEEE recommended practice and requirements for harmonic control in electric power systems (Revision of IEEE Std 519-1992); 2014. p. 1–29. DOI:10.1109/IEEESTD.2014.6826459.